INSTITUTE OF PHYSICS PUBLISHING and INTERNATIONAL ATOMIC ENERGY AGENCY NUCLEAR FUSION
Nucl. Fusion **42** (2002) 247–257 PII: S0029-5515(02)34651-9

# New insights into MHD dynamics of magnetically confined plasmas from experiments in RFX

**P. Martin[a], S. Martini, V. Antoni[a], L. Apolloni, M. Bagatin[a], W. Baker, O. Barana, R. Bartiromo, P. Bettini, A. Boboc, T. Bolzonella, A. Buffa[a], A. Canton[a], S. Cappello, L. Carraro, R. Cavazzana, G. Chitarin, S. Costa, F. D'Angelo, S. Dal Bello, A. De Lorenzi, D. Desideri, D. Escande[1], L. Fattorini, P. Fiorentin, P. Franz[a], E. Gaio, L. Garzotti, L. Giudicotti[a], F. Gnesotto, L. Grando, S.C. Guo, P. Innoccente, A. Intravaia[a], R. Lorenzini, A. Luchetta, G. Malesani, G. Manduchi, G. Marchiori, L. Marrelli, E. Martines, A. Maschio, A. Masiello, F. Milani, M. Moresco[a], A. Murari, P. Nielsen, M. O'Gorman, S. Ortolani, R. Paccagnella, R. Pasqualotto, B. Pégourié[2], S. Peruzzo, R. Piovan, N. Pomaro, A. Ponno[a], G. Preti[a], M.E. Puiatti, G. Rostagni, F. Sattin, P. Scarin, G. Serianni, P. Sonato, E. Spada, G. Spizzo[a], M. Spolaore[a], C. Taliercio, G. Telesca, D. Terranova[a], V. Toigo, L. Tramontin, M. Valisa, N. Vianello[a], M. Viterbo, L. Zabeo, P. Zaccaria, P. Zanca, B. Zaniol[a], L. Zanotto, E. Zilli, G. Zollino**

Consorzio RFX, Associazione Euratom–ENEA sulla Fusione, Padua, Italy
[1]CNRS–Université de Provence, Marseille, France
[2]Association Euratom–CEA sur la Fusion Contrôlée, CEA Cadarache, Saint-Paul-lez-Durance, France

E-mail: martin@igi.pd.cnr.it

Received 8 October 2000, accepted for publication 8 October 2001
Published 20 March 2002
Online at stacks.iop.org/NF/42/247

**Abstract**
The experimental and theoretical activity performed in the RFX device has allowed a deeper insight into the MHD properties of the reversed field pinch (RFP) configuration. A set of successful experiments has demonstrated the possibility of influencing both the amplitude and the spectrum of the magnetic fluctuations which characterize the RFP configuration. A new regime (quasi-single-helicity states) where the dynamo mechanism works in a nearly laminar way and a helical core plasma is produced has been investigated. With these studies a reduction of magnetic chaos has been obtained. The continuous rotation of wall locked resistive tearing modes has been obtained by an $m = 0$ rotating perturbation. This perturbation induces rotation of $m = 1$ non-linearly coupled modes.

**PACS numbers:** 52.30.-q, 52.55.Lf

## 1. Introduction

The search for advanced and innovative confinement scenarios is one of the major challenges in the studies on magnetic confinement of fusion plasmas. An important aspect in this task is the optimization of magnetic equilibrium and the understanding and control of MHD phenomena. MHD instabilities are often the origin of confinement degradation and/or sudden plasma termination. Many of their important properties depend on basic properties of the magnetic field configuration, and can be studied in several devices. To this extent, a well diagnosed large reversed field pinch (RFP)

[a] Also at: Istituto Nazionale di Fisica della Materia, UdR Padova, Padua, Italy.

experiment like the RFX device (major radius $R = 2$ m, minor radius $a = 0.46$ m) [1] represents an excellent test bench for many MHD studies, since these display a variety of features in RFP.

MHD instabilities are important in RFPs, as they break the toroidal symmetry of the magnetic field and drive the self-generation of the reversed toroidal magnetic field through a mechanism traditionally called the dynamo effect [2]. The RFP equilibrium in cylindrical co-ordinates is in fact characterized by a safety factor $q(r) = rB_\varphi(r)/RB_\vartheta(r)$ which is typically close to $a/2R$ in the plasma core and decreases to a slightly negative value at the edge. This means that the poloidal magnetic field in RFPs is of the same order of magnitude as the toroidal magnetic field. Moreover, sustainment of magnetic field reversal requires that there are poloidal electric currents in the plasma. These currents cannot be directly driven by the inductive toroidal electric field produced by the transformer effect, and a Lorentz 'dynamo-like' contribution $\boldsymbol{v} \times \boldsymbol{B}$ is therefore necessary. This implies the existence of a self-organized velocity field in the plasma, which couples to part of the magnetic field to produce the required electric field.

A series of numerical simulations [3–5] and experimental results (see, for example, Refs [2, 6] and the references quoted therein) have shown that the magnetic field and velocity fluctuations associated with MHD tearing modes provide a robust mechanism with which to produce a dynamo electric field. Owing to the shape of the $q$ profile, in fact, many tearing modes, resonant on closely spaced rational surfaces, can indeed be simultaneously destabilized. As a result, the instabilities generating the dynamo have, typically, a wide $k$ spectrum. Many $m = 0$ and $m = 1$ modes with different toroidal mode numbers $n$ and similar amplitudes are in fact simultaneously present in the standard multiple helicity (MH) RFP state. This is shown in Fig. 1, where typical MH $m = 0$ and $m = 1$ toroidal spectra measured in RFX are reported. The global normalized fluctuation amplitude is observed in RFX to scale with the magnetic Lundquist number $S$ as $b/B \propto S^{-0.16\pm0.02}$ [7], which is close to the output of numerical simulations [5]. These magnetic fluctuations destroy closed magnetic surfaces in the plasma core and induce magnetic chaos over large portions of the plasma volume. This produces a high transport in the radial direction and therefore spoils particle and energy confinement. Moreover, through phase locking of the modes, a toroidally localized distortion of the magnetic equilibrium and a bulging of the plasma are produced. When modes also lock to the wall in a particular toroidal position, for example, because of field errors, this results in a strong plasma–wall interaction [8]. This latter feature, despite the different origin, is shared with other toroidal configurations.

The study of the mechanisms driving MHD instabilities and of the techniques to control them is therefore crucial for RFP research, both for understanding the basic physics underlying the configuration and for assessing its fusion perspectives. A substantial amount of work has been done within the RFP community on this subject. In particular, a major effort has been performed in the RFX device. RFX has, in fact, among the other RFP devices, unique features in terms of plasma current, geometrical size and diagnostic capabilities. RFX is the largest RFP device nowadays in operation and is where the highest plasma current has been achieved (1.1 MA).

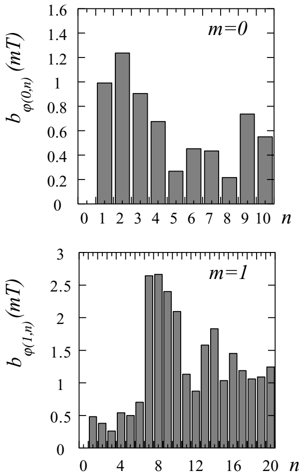


**Figure 1.** Typical $m = 0$ and $m = 1$ toroidal spectra for an MH RFX plasma. The $k$ spectrum of MHD modes is wide in this condition.

Moreover, a significant number of diagnostics, including several profile diagnostics, enable efficient monitoring of the plasma dynamics.

In this article we describe therefore the main recent theoretical and experimental results on MHD studies obtained in RFX. Our purpose is to guide the reader along a path that, starting from a standard RFP plasma,

(a) Presents a more updated understanding of relevant experimental and theoretical aspects of MHD physics in RFPs,
(b) Describes the results of effective techniques for the control of MHD instabilities,
(c) Indicates possible guidelines for confinement performance improvement,
(d) Describes the modifications to the RFX device that allow it to cope better with the problem of active interaction with the MHD phenomena.

Experiments and theory in RFX have in fact been directed towards the analysis of MHD mode dynamics, of the non-linear coupling between modes, of the transitions between turbulent and laminar dynamo regimes, of the process underlying mode locking and of the techniques devoted to the control of magnetic turbulence and to the induction of wall locked mode active rotation.

To fulfil our aim the article is organized as follows: Section 2 is dedicated to results about the turbulent (MH) RFP dynamo and in particular to the behaviour of $m = 0$ and $m = 1$ modes and to their influence on confinement, and to the analysis of phase locking of tearing modes. Sections 3, 4 and 5 contain a description of the experimental and theoretical results concerning a new self-organized laminar dynamo regime, i.e. the quasi-single-helicity (QSH) regime. In Section 6 we will present the new techniques for active control of magnetic fluctuations which have been successfully developed in RFX. Future directions for work in the RFX device are the subject of Section 7, and conclusions are drawn in Section 8.

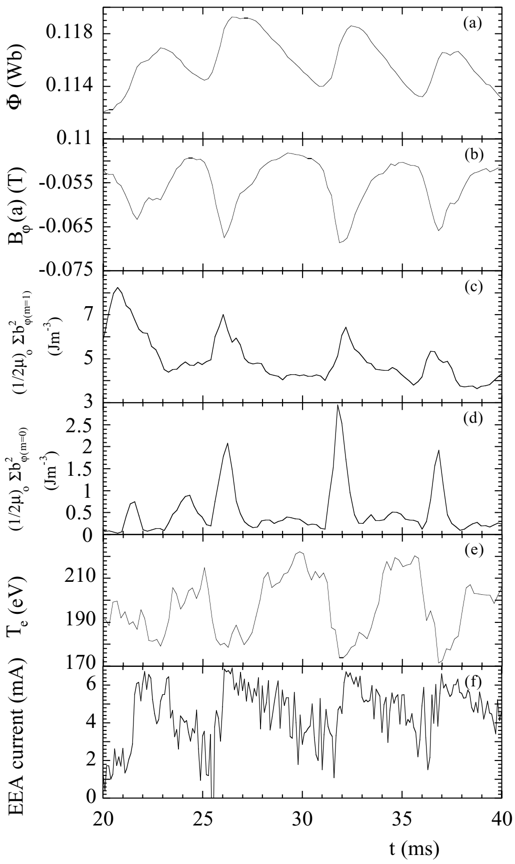


**Figure 2.** A sequence of discrete dynamo events during RFX discharge 7423. (a) Magnetic toroidal flux $\Phi$. Periodic flux generation events are evident. (b) Magnetic toroidal field at the wall $B_\varphi(a)$. (c) Total magnetic volume energy density stored in the $m = 1$ modes with $n = 7$–14. (d) Total magnetic volume energy density stored in the $m = 0$ modes with $n = 1$–5. (e) Core electron temperature $T_{e0}$. (f) Electron energy analyser collector output current (proportional to the suprathermal electron flux at the plasma edge).

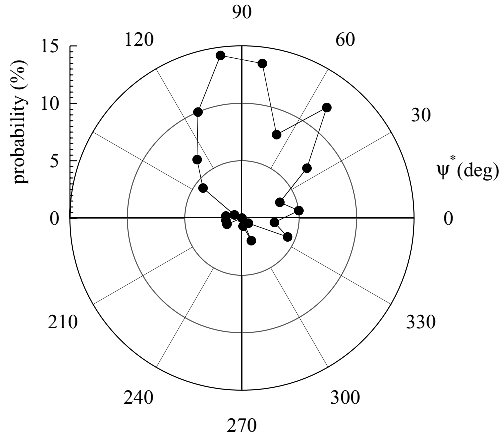


**Figure 3.** Polar plot of the probability distribution for the three mode phase differences defined as $\psi^* = \psi^{1,n+i} - \psi^{1,n} - \psi^{0,i}$ ($i$ = 1–4). For each angle $\psi^*$ the point gives the probability of that angle. The ensemble is formed of 140 measurements.

## 2. The RFP turbulent dynamo

Self-organization processes have been observed since the very beginning of RFP experimental activity [9, 10]. In fact, independently from the initial conditions, the state with a reversed toroidal field is reached spontaneously and maintained with enough applied toroidal voltage against resistive diffusion. It is the plasma that provides the conversion of the supplied poloidal magnetic flux into toroidal magnetic flux through a self-organization mechanism traditionally called a dynamo. The dynamo operates because of plasma MHD instabilities: the basic mechanism of relaxation and field reversal generation has been recognized in the non-linear evolution of an $m = 1$ resistive kink instability in the presence of an externally applied toroidal electric field [3, 11–13]. As a result the RFP dynamics is governed by current sheet reconnection [5]. This MHD picture of the MH (or turbulent) field generation mechanism is based on rather convincing evidence, in particular in those cases where the dynamo acts in discrete events, such as those shown in Fig. 2. During the discharge reported in this figure periodic and macroscopic toroidal field generation events are visible, as shown by the magnetic toroidal flux $\Phi$ and the edge magnetic toroidal field $B_\varphi(a)$ waveforms (Figs 2(a) and (b), respectively). The generation of an average magnetic toroidal flux is associated with an increase of toroidal field reversal. During these events sudden bursts of magnetic fluctuation energy are recorded. Figures 2(c) and (d) show the global energies of the $m = 1$ and $m = 0$ modes, respectively. Both of them peak as magnetic flux is generated. As a result of the increased magnetic chaos generated by these modes, the hot plasma core is short-circuited with the cooler edge and there is a significant increase of energy loss, as indicated by the sudden crash of the core electron temperature trace shown in Fig. 2(e). During these discrete macroscopic events a growth of the suprathermal electron flow measured at the plasma edge by an electrostatic energy analyser is observed (Fig. 2(f)). This enhanced suprathermal electron flow is consistent with the acceleration of those particles in the current sheets generated during the reconnection events triggered by the increased MHD activity [5] and also with the classical Spitzer–Harm distortion of the Maxwellian distribution function. This latter picture is also supported by a recent investigation of the trajectory deflection of frozen hydrogen pellets launched into the RFX plasma [14]. This study has allowed diagnosis of the suprathermal electrons in the plasma and, to this end, the electron distribution function. The results of Ref. [14] indicate that the pellet trajectory can be described using the classical Spitzer–Harm distortion of the Maxwellian distribution function caused by the MHD dynamo electric field. This provides further confirmation that a dynamo mechanism based on a local mean field electrodynamics theory can account for the observed magnetic field.

The $m = 0$ and $m = 1$ resistive tearing modes driving the RFP dynamo are found to be systematically phase locked in RFX. They determine a toroidally localized non-axisymmetric perturbation called the locked dynamo mode (LDM). The LDM is always locked to the wall in RFX so that the perturbation is stationary in the laboratory frame. In a recent analytical formulation [15, 16] the LDM is described as the result of the non-linear interaction between the $m = 0$ and $m = 1$ modes. Moreover, this theory predicts that under locking conditions the phase difference of the interacting $m =$

0, 1 modes belongs to one of the two intervals $[-\pi/4, \pi/4]$ or $[3\pi/4, 5\pi/4]$. We have studied the experimental phase relation between the $m = 1$ and $m = 0$ modes that are involved in the locked mode phenomenology of RFX. Assuming for the perturbed quantities the standard tearing mode definitions [15, 17], we find that the phase differences between the $m = 1$ and $m = 0$ modes follow the relation $\psi^{1,n+i} - \psi^{1,n} - \psi^{0,i} = \psi^*$, with $\psi^*$ distributed over a rather large interval ranging between $\approx 0$ and $\approx 135°$ [18]. $\psi^{1,n}$ is the phase of the $(m = 1, n)$ mode and $\psi^{0,i}$ is the phase of the $(m = 0, i)$ mode. The results are displayed in Fig. 3, which shows in a polar plot the frequency distributions of the measured $\psi^*$ values that are spread over a wide range. The RFX experimental results are therefore not consistent with the theoretical prediction of $\psi^* \in [-\pi/4, \pi/4]$ or $\psi^* \in [3\pi/4, 5\pi/4]$. This discrepancy could be due to the theoretical assumption [15] that the $m = 0$ modes are intrinsically stable, which implies that they are generated only by the non-linear interaction of the dominant $m = 1$ perturbations. This assumption possibly holds true for plasmas bounded by a close fitting conducting shell, as indicated for example by 3-D MHD numerical simulations. The actual RFX situation is different, since the conducting shell is about 8 cm distant from the plasma, which corresponds to a ratio between the shell and the plasma radii of about 1.2. In this case a linear MHD stability analysis [17] indicates that the RFX boundary condition should correspond to unstable $m = 0$ modes. The measured $m = 0$ modes in RFX are therefore likely to be the outcome of two processes: linear instability and non-linear coupling of $m = 1$ modes. This latter process is possibly the most important one when there is more need of a turbulent dynamo, as during the discrete dynamo events shown in Fig. 2. To summarize, we find that the MH state in RFX is consistent with the MHD dynamo with the inclusion of an $m = 0$ mode both linearly and non-linearly driven.

## 3. Experimental results on QSH states

Recent experimental measurements in RFX [19–21] have shown that a new MHD dynamo regime is present, where magnetic field topology can be rather different from that observed in the standard wide spectrum MH case. In this regime, dubbed the quasi-single-helicity (QSH) regime, the $m = 1$ magnetic field fluctuation spatial spectrum is dominated by one individual $(m = 1, n \approx 2R/a)$ MHD mode. In this case the symmetry breaking required to have a stationary RFP equilibrium in a resistive plasma is provided by the saturation of a resistive kink mode. This is different from the helical state predicted by Taylor [22].

QSH states are reproducibly obtained in RFX either transiently (for several milliseconds) or in stationary conditions (i.e. during the whole pulse duration) [20]. Figure 4 illustrates the difference between an MH and a QSH plasma in terms of MHD modes. The two plasmas have similar global parameters, but in the QSH case the predominance of the $(m = 1, n = 8)$ mode is evident. On the contrary in the MH case all the $m = 1$ modes between $n = 7$ and $n = 12$ have comparable amplitudes, within a factor of 2. To quantify the difference between the two spectra it is convenient to introduce a measurement of the 'width' in the toroidal mode number $n$

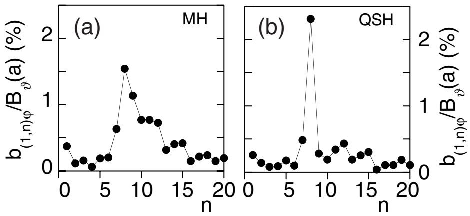


**Figure 4.** Toroidal spectra of $m = 1$ magnetic modes for (a) an MH plasma (discharge 11392, $t = 44.5$ ms) and for (b) a QSH plasma (discharge 11392, $t = 34.5$ ms).

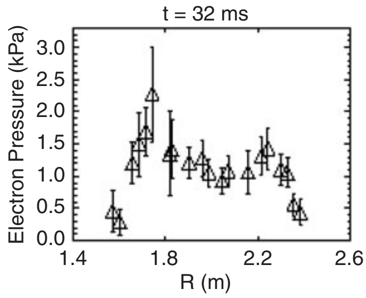


**Figure 5.** Radial electron pressure profile during a QSH state.

of the $m = 1$ spectrum. This is done using the spectral spread, $N_s$ defined as

$$N_s = \left[ \sum_n \left( \frac{W_{n,\varphi}}{\sum_m W_{m,\varphi}} \right)^2 \right]^{-1}$$

[23], where $W_{n,\varphi}$ is the energy of the $(m = 1, n)$ mode. $N_s$ is an indicator of the effective number of $n$ modes composing the spectrum. A pure single helicity (SH) spectrum has $N_s = 1$. For the cases shown in Fig. 4 we have $N_s \approx 3.7$ for the MH plasma and $N_s \approx 1.2$ for the QSH state. The exploration of the plasma core reveals that a different magnetic topology is associated with QSH states. The imaging of the plasma core, obtained through soft X ray (SXR) tomography [21], shows a poloidally symmetric emissivity in the MH state. In contrast a 'bean'-like hot $m = 1$ structure is evident in the QSH case. While a relatively small $m = 1$ component in the SXR emissivity profile is present in the MH state, mostly due to the Shafranov shift, in the QSH case there is a $m = 1$ component, radially localized and of the same order of magnitude as the $m = 0$ component [20]. The location of the $m = 1$ island systematically coincides with the resonance radius and poloidal phase angle of the dominant $m = 1$ magnetic mode. This evidence suggests that helically symmetric closed magnetic surfaces are generated.

The improvement of the magnetic flux surfaces in the plasma core is proven also by direct electron temperature and density profile measurements performed by multipoint Thomson scattering, which indicate that this helical structure confines a higher pressure than the plasma nearby [19, 21]. A pressure profile, measured for the first time in an RFP, taken during a QSH state is shown in Fig. 5. We note the radial asymmetry of the profile corresponding to the increased pressure into the helical coherent structure. Indeed helical hot regions where the electron temperature can be more than 50% higher than the neighbouring bulk plasma are systematically observed in RFX during QSH states.

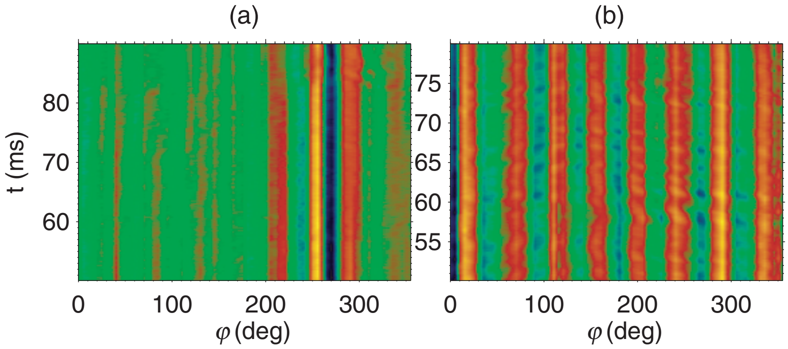


**Figure 6.** Time evolution of the profile along the toroidal angle $\varphi$ of the energy stored in the global magnetic perturbation of the edge toroidal field $b_\varphi^2$ for (a) an MH plasma and for (b) a QSH stationary plasma. The red stripes alternate with green stripes in the QSH case indicating a modulation with toroidal mode number $n = 8$, whereas in the MH case a magnetic perturbation localized in space is evident.

The onset of a QSH state has relevant consequences not only for the plasma core, but also for the edge and for the plasma–wall interaction [24] due to LDM. Figure 6 compares the time evolution of the profile, measured along the toroidal angle $\varphi$, of the energy stored in the global magnetic perturbation of the edge toroidal field $b_\varphi^2$ for an MH plasma and for a QSH stationary plasma. The red stripes alternate with green stripes in the QSH case indicating a modulation with the toroidal mode number $n = 8$, whereas in the MH case a magnetic perturbation localized in space is evident (as expected because of the wide spectrum in $k$ space, due to the large number of toroidal $m = 1$ modes). The decrease in the toroidal localization of the plasma bulge in the QSH case is evident. Effects on the plasma–wall interaction are also described with the help of Fig. 7, where the effects of MHD modes on the LCFS in MH and QSH plasmas are discussed. The displacement $\Delta(\varphi)$ of the LCFS versus the toroidal angle in MH conditions is shown in Fig. 7(a). $\Delta(\varphi)$ is reconstructed from magnetic measurements [25]. In the toroidal region where modes lock to the wall $\Delta(\varphi)$ is almost 4 cm. Figure 7(b) shows the horizontal component of the displacement $\Delta_h(\varphi)$, which also has a well pronounced maximum. This perturbation produces a localized plasma–wall interaction, whose typical signature is a significant local increase of the total radiation emissivity, which in some cases can reach extremely high values (up to 100 MW/m$^3$) [26]. In principle, if we had a pure SH state such as that predicted by numerical simulations [27], the plasma would assume a helical shape. The displacement of the LCFS would therefore be constant as a function of the toroidal angle $\varphi$ and indeed there would by no localized perturbation at all. In fact, in experimental QSH cases we do not obtain a pure SH state and the 'secondary' modes have non-zero amplitude. Nonetheless, the maximum displacement $\Delta(\varphi)$ changes significantly in QSH states: Fig. 7(c) indicates that when the plasma is in a QSH state the $\Delta(\varphi)$ function does not show a pronounced maximum and it is more uniform, oscillating around a pedestal due to the helical distortion associated with the dominant $m = 1$ mode. The dominant $n = 8$ modulation is evident in the $\Delta_h(\varphi)$ waveform, shown in Fig. 7(d).

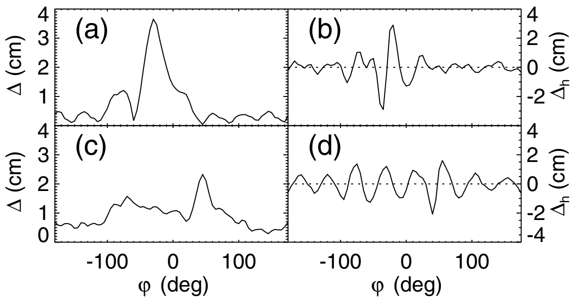


**Figure 7.** Maximum displacement $\Delta(\varphi)$ of the LCFS and its horizontal component $\Delta_h(\varphi)$ versus the toroidal angle $\varphi$ for an MH state (discharge 13250, $t = 55$ ms) (frames (a) and (b)) and for a QSH state (discharge 11407, $t = 36$ ms) (frames (c) and (d)).

## 4. Theoretical aspects of single helicity

Toroidal field reversal implies the loss of axisymmetry. This is easily shown for a cylindrical RFP. Indeed if cylindrical symmetry is assumed, the parallel Ohm's law implies that the reversal of the toroidal field means the reversal of the parallel current. As, according to Ampère's law, the azimuthal component of the current is the opposite of the radial derivative of the axial field, current reversal implies that the axial field is a minimum at its reversal point, which is self-contradictory. It is interesting to note that the Cowling theorem [28] has been traditionally invoked to explain why an axisymmetric RFP is impossible. This theorem states that axisymmetric magnetic fields cannot be maintained by axisymmetric dynamo action, i.e. by a given axisymmetric velocity field. This theorem does not apply to stabilized $Z$ pinches, since non-axisymmetry of the magnetic field is not a general rule as for the kinematic dynamo: it is not necessary for the paramagnetic pinch, but it is for the RFP. Indeed the kinetic energy of these pinches is much smaller than their magnetic energy, their velocity field is not directly driven, and the poloidal part of their field is naturally provided through the forced toroidal (axial) current. For the RFP a deformation of the plasma with at least one helicity must be present. The kink instability is the natural origin of this deformation since $q < 1$.

The possibility of having an RFP plasma in a pure SH state has been put forward since 1983 through two dimensional numerical simulations [29–33] where a stationary RFP state was found by forcing SH. The SH states have a laminar dynamo produced by a single mode and its harmonics and correspond to a magnetic field with good flux surfaces, a feature favourable to good confinement. They are not Taylor states, since the sign of their helical pitch is opposite to that in Taylor's theory [22]. In fact, an intuitive description of the magnetic field self-reversal process allows the SH state to be viewed as the non-linear state of a resistive kink mode self-stabilized by outer toroidal field reversal, if toroidal flux conservation is imposed in the relaxation process [34]. In a tokamak the stabilization of the $m = 1$ kink mode is made possible by the plasma itself because the helical deformation it drives costs energy in the whole $q > 1$ domain. No such mechanism is available in the RFP where $q < 1$ everywhere, and outer field reversal is necessary to stabilize the kink mode.

The loss of axisymmetry of the magnetic surfaces induces a modulation of the current density along the field lines. This modulation is driven by an electrostatic field produced by charge separation. This electric field and the induction electric field produce an $\boldsymbol{E} \times \boldsymbol{B}$ velocity field which is the dynamo velocity field of the RFP [34]. Therefore the origin of the dynamo in the SH state of the RFP is a simple consequence of the pinch effect and of the breaking of axisymmetry due to the resistive kink mode: the helical magnetic equilibrium has an electrostatic helical counterpart which provides the helical part of the dynamo velocity field, a slave laminar field. This picture is the physical interpretation of the scheme proposed in reference [35] for the calculation of SH states. The SH ohmic states of the RFP have been studied in the framework of the resistive MHD model in cylindrical geometry with and without pressure [35–37]. (In relation to Ref. [36], see also p. 114 of Ref. [2].) In the force-free case we solved the Grad–Shafranov equation in helical co-ordinates by assuming a polynomial dependence of $\lambda = \boldsymbol{J} \cdot \boldsymbol{B}/B^2$ on the helical flux function $\chi$. This equation is found to have two basins of solution: in the first one the axisymmetric part of the helical flux function $\chi_0$ has a local maximum in the plasma region (at the resonance radius), while $\chi_0$ is a monotonic function of $r$ in the second one. The two basins correspond to a resonant or non-resonant helical term, respectively. When the pressure is taken into account a polynomial dependence of

$$\tilde{\lambda} = \boldsymbol{J} \cdot \boldsymbol{B}/B^2 - p'g/B^2$$

on the helical flux function $\chi$ is assumed, where $p$ is the pressure, $p' = dp/d\chi$ and $g = mB_z - krB_\vartheta$ is the helical magnetic field; the pressure is assumed to depend linearly on the helical flux function $p(\chi) = p_0 + p_1\chi$, where $p_0 = -p_1\chi_0(a)$ since $p$ must vanish at the plasma boundary. It is then possible to find ohmic solutions where $\langle B_z \rangle$ (axial magnetic field averaged over the helical flux surface) does not reverse in the outer plasma region, while the axisymmetric field $B_z^{(0,0)}$ does (Fig. 8); $\lambda$ is found to be almost constant far from the edges. The corresponding poloidal contour plot of the helical flux function

$$\chi(r, u) = \chi_0(r) + \chi_1(r) \cos u$$

in a poloidal section shows a bean shaped helical structure in the plasma core, rather similar to that experimentally observed.

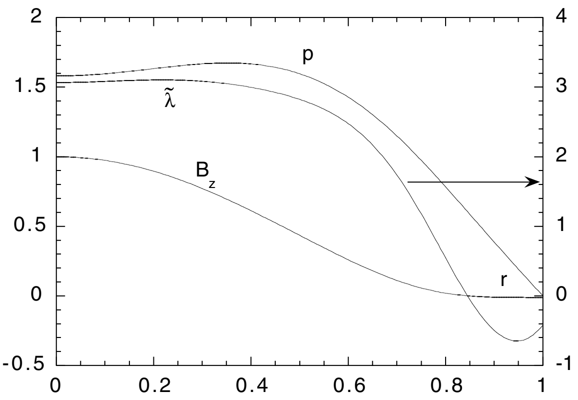


**Figure 8.** $B_z^{(0,0)}$, $\tilde{\lambda}$ and $p$ ($p$ amplified by a factor of 60) as functions of $r$ for $\Theta = 1.78$, $F = -0.06$ and a volume averaged $\beta = 0.1$, where $\Theta = B_\theta(a)/\langle B_\varphi \rangle$ and $F = B_\varphi(a)/\langle B_\varphi \rangle$ are the usual pinch and reversal parameters for RFP configurations ($\langle \ldots \rangle$ denotes the cross-sectional average).

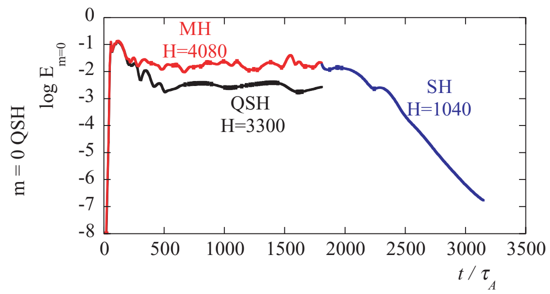


**Figure 9.** Time evolution of the magnetic energy stored in $m = 0$ MHD modes, $E^M_{m=0}$, for three different numerical simulations corresponding to an MH regime (red curve), a QSH regime (black curve) and to a pure SH regime (blue curve). The value of the Hartmann number $H$ for each simulation is shown in the plot.

The RFP dynamics is studied with a simple viscoresistive MHD model [5,38]:

$$\frac{\partial \boldsymbol{B}}{\partial t} = \boldsymbol{\nabla} \times (\boldsymbol{v} \times \boldsymbol{B}) - \boldsymbol{\nabla} \times (\eta \boldsymbol{J}) \tag{1}$$

$$\frac{\partial \boldsymbol{v}}{\partial t} + (\boldsymbol{v} \cdot \boldsymbol{\nabla})\boldsymbol{v} = \boldsymbol{J} \times \boldsymbol{B} + \boldsymbol{\nabla}^2(\nu \boldsymbol{v}) \tag{2}$$

with $\boldsymbol{J} = \boldsymbol{\nabla} \times \boldsymbol{B}$ and $\boldsymbol{\nabla} \cdot \boldsymbol{B} = 0$. Here time and velocity are normalized to the Alfvén time and velocity, respectively, and the other variables to macroscopic values: in these units $\eta$ is the inverse Lundquist number $\eta = \tau_A/\tau_R \equiv S^{-1}$ and $\nu$ corresponds to the inverse magnetic Reynolds number, $\nu = \tau_A/\tau_V \equiv R^{-1}$, for a scalar kinematic viscosity.

A transition from MH to SH has been known to occur in this model when viscosity increases at fixed $S$ [5,35,38,39]. A recent scaling approach to this model reveals that the Prandtl number acts only through the inertia term [39]. When this term is negligible the dynamics is ruled by the Hartmann number $H = (\eta/\nu)^{-1/2}$ only. This occurs for the dynamics of the RFP, as shown by 3-D numerical simulations of the model. Therefore it is interesting to revisit the SH/MH transition with $H$ as the unique control parameter. An order parameter for the transition can be found by noticing that $E^M_{m=0}$, the magnetic energy of the $m = 0$ mode, vanishes in SH states due to the

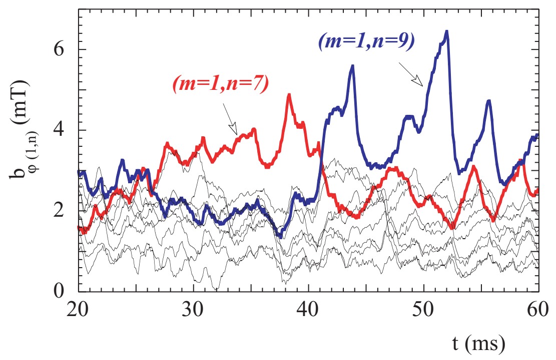


**Figure 10.** Time evolution of the $m = 1$ modes with $n = 7$–16 for RFX discharge 9712. Switching between two QSH states with different dominant modes ($n = 7$, red curve; $n = 9$, blue curve) is evident. An MH phase is present between the two QSH regimes. This experiment is reminiscent of the intermittent behaviour observed in numerical simulations [40] close to the bifurcation critical point.

lack of coupling of different $m = 1$ modes. In the MH state, on the contrary, $E^M_{m=0}$ remains at a finite, nearly constant, value throughout the discharge. This is shown in Fig. 9, where the time evolution of $E^M_{m=0}$ is displayed for three different plasma regimes. In the MH simulation, obtained with $H = 4080$, $E^M_{m=0}$ is almost flat in time until $t/\tau_A \approx 1800$ ($\tau_A$ is the Alfvén time). From this point on, the simulation is advanced with $H = 1040$ and the plasma enters an SH state. We note the exponential decay towards zero of $E^M_{m=0}$. An intermediate behaviour is observed in the QSH case, which is obtained starting the simulation with $H = 3300$. In this case after an initial exponential decay $E^M_{m=0}$ changes slope and ends on a plateau value, though much smaller than the MH case. This evidence is summarized by plotting $E^M_{m=0}$ versus $H$: a sharp transition around $H \approx 2500$ is found [40]. When $H$ is small, the system remains in an SH state and two basins of SH are shown to coexist. In the vicinity of $H = 2500$ the system displays a temporal intermittency whose laminar phases are of QSH type. For higher $H$ values the system reaches an MH state whose features, in particular magnetic chaos, are analogous to the traditional turbulent state of RFP plasmas. The result is seen to be independent of the Lundquist number $S$.

The intermittent behaviour of QSH states obtained in numerical simulations around the critical value of $H$ is consistent with experimental observations. The switching of the dominant toroidal mode number found in numerical simulations, discussed in [40], is also observed in the experiment. An example is shown in Fig. 10, where a QSH state with a dominant (1,7) mode is momentarily interrupted by an MH phase and then restarted but with a different geometrical helicity, which in this case is (1,9).

The SH–MH transition is analogous to a second order phase transition, where $E^M_{m=0}$ is the order parameter and $H$ the control parameter, and where the intermediate QSH regime corresponds to the critical divergence of the correlation scales. This approach raises the difficult issue of the definition of viscosity in magnetic fusion plasmas. The importance of $H$ in fusion physics has been raised previously in Refs [41–44].

A final point concerns the resilience to chaotic perturbations of a one parameter one degree of freedom Hamiltonian dynamics, which increases when its corresponding separatrix vanishes due to a saddle–node bifurcation. This is important for the magnetic chaos of QSH states of the RFP [45]. Indeed for a high enough amplitude of a resonant SH mode, the magnetic separatrix of this mode bifurcates out, which makes this SH mode more resilient to the chaos induced by the smaller modes with other helicities of the QSH state [45]. This supplies a rationale for the confinement improvement of helical domains found experimentally for QSH plasmas [20]. Such a feature would not be expected from the classical resonance overlap picture, as the separatrix disappearance occurs when the amplitude of the dominant mode increases.

## 5. The aspect ratio issue

Starting from the evidence of the shrinking of the $m = 1$ mode toroidal spectrum in QSH states, an analysis of the shape of the $m = 1$ mode behaviour as a function of the aspect ratio $R/a$ has been performed. Simple equilibrium considerations indicate in fact that, as the aspect ratio is decreased,

(a) The innermost resonant mode scales with the aspect ratio as $n \approx 2R/a$, since in the RFP

$$q(0) \approx \left(\frac{1}{2} - \frac{2}{3}\right)\frac{a}{R} \approx \frac{1}{n}$$

(b) The resonance surfaces of the $(1, n)$ modes are more widely spaced.

In addition to that, numerical simulations indicate that fewer toroidal modes contribute to the $m = 1$ spectrum as $R/a$ becomes smaller. This is shown, for example, in Fig. 11, where we report the spectra of $m = 1$ modes, obtained with the Specyl code [5], at a fixed $S$ value equal to $S = 3.3 \times 10^3$ for three values of the aspect ratio ($R/a = 1.2$, 2, 4). The effective number of modes $N_s$ in the spectra takes the following values: $N_s(R/a = 1.2) \approx 3$, $N_s(R/a = 2) \approx 3.2$, $N_s(R/a = 4) \approx 8.2$. This result is in agreement with the scaling laws presented in Ref. [23]. The RFX data in MH conditions follow these scaling laws, as $N_s$ typically ranges between 4 and 10. These results suggest that in an RFP at low aspect ratio a simpler mode structure might be present and the achievement of QSH might be facilitated.

## 6. Active control of MHD modes

As discussed in Section 2, the many MHD modes acting simultaneously in an MHD dynamo lock in phase and in RFX also to the wall, thus producing a stationary magnetic perturbation and a toroidally localized plasma–wall interaction (Figs 6 and 7). To overcome this problem, experiments on the active control of the MHD modes with a rotating external perturbation [46, 47] have been extensively pursued and the physical mechanism of mode interaction with external fields has been analysed. This allowed us to develop an operational strategy to produce active rotation of the LDMs through the current flat-top phase.

Active rotation of the modes is obtained with the rotating toroidal field modulation (RTFM) technique [46], through current modulation in the 12 sectors of the toroidal winding [48]. In this way a rotating toroidally localized $m = 0$

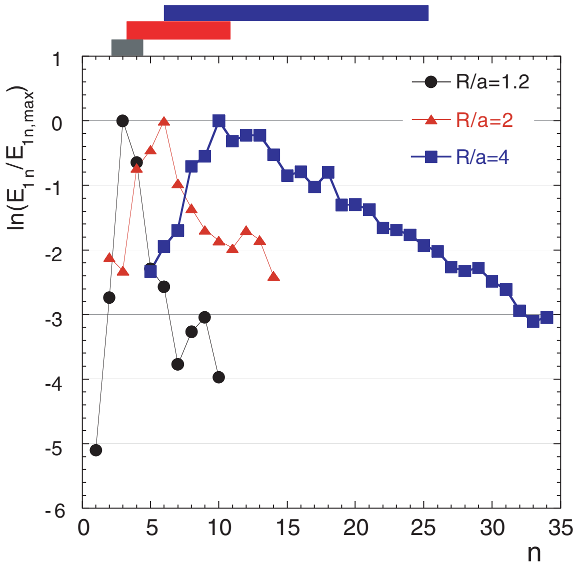


**Figure 11.** $m = 1$ spectra for different aspect ratios from numerical simulations (circles, $R/a = 1.2$; triangles, $R/a = 2$; squares, $R/a = 4$). The bars on the top of the figure give an indication of the width of the spectra.

perturbation of the toroidal field is applied to the plasma. The rotating perturbation is most effective if its rotation frequency is $\omega < 35$ Hz and its toroidal mode content is mainly $n = 1$. When continuous rotation sets in, the LDM rotates with a toroidal velocity equal to the driving perturbation and the latter leads the LDM by an angle of less than $\pi/2$. An example of the results obtained with this technique is shown in Fig. 12, where the time evolution of the LCFS maximum displacement profile along the toroidal co-ordinate is reported for a discharge without an RTFM (Fig. 12(a)) and for one with an RTFM (Fig. 12(b)).

The observed LDM behaviour can be explained by the interaction of the external field with the tearing modes. The basic interaction is between the external $m = 0$ perturbation and the internally resonant $m = 0$ mode. Then the effects are transferred to the $m = 1$ internally resonant modes due to the non-linear three wave interaction mechanism which underlies the LDM [49]. In particular, the external $m = 0$ magnetic field interacts with the plasma inducing a sheet current at the resonant surface that is the field reversal surface at $r = r_0$. The current is proportional to the radial component of the external field $B_r^{0,1}(r_0)$. In this way, an electromagnetic torque is exerted on the $m = 0$ mode given by

$$T_{ext,z}^{0.1} \propto b_r^{0.1} B_r^{0.1}(r_0) \sin(\Delta\psi) \tag{3}$$

where $b_r^{0,1}$ is the radial field associated with the width of the magnetic island generated by the (0,1) mode and $\Delta\psi$ is the phase shift between the mode and the perturbation. In (3) only the toroidal component $T_{ext,z}^{0,1}$ is considered, because of the strong damping of the poloidal rotation in a torus. In order to induce rotation of the LDM, $T_{ext,z}^{0,1}$ must be high enough to overcome the braking torque on the $m = 0$ mode due to static error fields. Once that is true, the $m = 0$ mode can hook up to the applied perturbation. To this end a balance must be reached between the drag torque due to plasma viscosity and

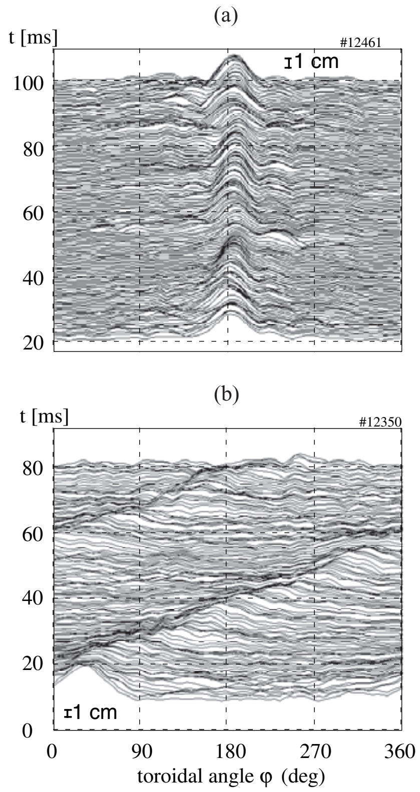


**Figure 12.** Time evolution of the LDM: the radial displacement of the plasma surface on the poloidal plane as a function of toroidal angle is shown during the current flat-top for (a) a standard discharge and (b) a discharge with RTFM.

eddy currents in the vessel [16] (both proportional to $\omega$) and $T_{ext,z}^{0,1}$. This means that $\Delta\psi$ saturates at a value in the interval 0–$\pi/2$, i.e. in the stable range where the applied torque is an increasing function of $\Delta\psi$.

The applied torque $T_{ext,z}^{0,1}$ is transferred to the $m = 1$ modes via the non-linear coupling. For any pair of $m = 1$ modes with toroidal numbers $n$ and $n + 1$, the torque due to the three wave interaction with the $m = 0$ mode are in fact given by [50]:

$$T_z^{0.1} \propto C_n \sin(\psi^{1,n+1} - \psi^{1,n} - \psi^{0.1}) = C_n \sin(\Delta\psi^{3w}) \tag{4a}$$

$$T_z^{1,n} \propto nC_n \sin(\psi^{1,n+1} - \psi^{1,n} - \psi^{0.1}) = nC_n \sin(\Delta\psi^{3w}) \tag{4b}$$

$$\begin{aligned} T_z^{1,n+1} &\propto -(n+1)C_n \sin(\psi^{1,n+1} - \psi^{1,n} - \psi^{0.1}) \\ &= -(n+1)C_n \sin(\Delta\psi^{3w}) \end{aligned} \tag{4c}$$

where $C_n$ is a coefficient proportional to the amplitude of the modes and to their overlap integral, $\psi^{m,n}$ is the phase of the $(m, n)$ mode and $\Delta\psi^{3w} = \psi^{1,n+1} - \psi^{1,n} - \psi^{0.1}$. It is seen that the torque on the $m = 1$ modes is larger than that on the $m = 0$ mode by a factor $n$ (with $n > 7$ for a typical spectrum in RFX). Such a leverage effect is responsible for the fact that the electromagnetic torque given by (2) is strong enough to maintain the phase locking of all of the $m = 1$ modes (i.e. to hold $\Delta\psi^{3w} \approx$ const) both in standard discharges and in those with active mode rotation. In the latter cases the external perturbation induces a linear rate of change of

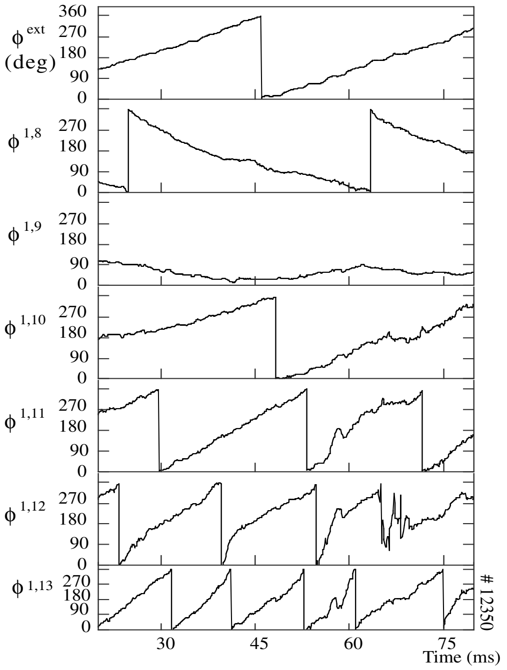


**Figure 13.** Phases of the externally applied magnetic perturbation and of the $m = 1$ modes with $n = 8$–13 for a discharge with RTFM. The (1,8) mode travels backwards and the rotation frequency increases with $n$ for $n > 10$.

$\psi^{0,1}$, hence the phase locking condition requires either $\psi^{1,n}$ or $\psi^{1,n+1}$ to follow the rotation: it is a dynamic equilibrium where the action of $T^{0,1}_{ext,z}$ rotates both the $m = 0$ mode and one of the $m = 1$ modes (the one subject to less braking torque). The other $m = 1$ mode remains stationary because of the phase locking condition which makes $\Delta\psi^{3w}$ saturate at a value such that the torque given by (2) is just sufficient to match the braking torque on the rotating $m = 1$ mode. Iterating the scheme for all of the $[n; n+1]$ couples of modes one sees that the $m = 1$ mode subject to the highest braking torque can never be hooked up by the perturbation, hence its phase remains stationary. Such a mode is typically the one with the largest amplitude, for example, the $n = 9$ mode in Fig. 13. The condition $\Delta\psi^{3w} \approx$ const also implies that the mode with $n = n_{stat} + 1$ must co-rotate with the external perturbation, whereas the one with $n = n_{stat} - 1$ has to go backward. $n_{stat}$ is the toroidal mode number of the mode which remains stationary. Moreover, the next adjacent $m = 1$ mode $n = n_{stat} + 2$ must rotate relative to the $n = n_{stat} + 1$ mode, i.e. it moves at $2\omega$ in the laboratory frame; and so on for modes with higher or lower $n$. All the above features are found in the example shown in Fig. 13, which is remarkable evidence of the non-linear coupling underlying the LDM.

The recipe to obtain mode rotation through the current flat-top entails enforcing a toroidal position of the LDM during the current rise phase by applying a stationary $m = 0$ perturbation, which acts as a seed for mode locking. Then the RTFM is applied with an initial phase which satisfies the $\Delta\psi < \pi/2$ condition. The reliable rotation of the locked modes constitutes a major step towards routine operation at high currents in RFX, with good control of particle recycling and of plasma density [51]. Carbon blooming, a typical consequence of earlier high current operation, is avoided by spreading the heat load on the first wall. The driving field required for rotation increases with plasma current and density, and with rotation frequency. The last relationship is readily understood in terms of the linear dependence of the drag torque on $\omega$. The density dependence is probably due to the associated effect on the temperature, and hence on the drag torque linked to plasma viscosity. Finally, the current scaling could be due to the decrease of the amplitude of the $m = 0$ modes which show a scaling stronger than the $m = 1$ ones. With the present power supplies, a rotation frequency of 20 Hz is obtained up to the density limit for current below the megamp level, whereas in discharges with plasma current $\approx$1–1.2 MA active mode rotation is possible only at 10 Hz and with density corresponding to an $I/N$ parameter of $3 \times 10^{-14}$ A m.

## 7. Future directions

The results presented in this article, together with the existing literature, indicate that the next step in the RFP experimental and theoretical research should be aimed at exploiting the full synergy between the various techniques discussed. All these techniques are directly or indirectly linked to the crucial issue of MHD instability active control. This in fact appears to be one of the major factors in determining the fusion relevance of the RFP configuration. It is expected that this could be realized by the simultaneous action of a large number of active coils which produce harmonic magnetic and electric fields in the outer plasma region, also by means of feedback techniques. This has the goal of substantially improving the capability of interacting with MHD modes.

To this end the magnetic front end of the RFX device is undergoing substantial modification, with the principal aim of extending the MHD studies along the new paths opened by the recent results. This will be accomplished by the new components of the magnetic system consisting of a thinner and closer shell ($\tau_s \approx 50$ ms, $b/a \approx 1.1$ compared with the old $\tau_s \approx 400$ ms, $b/a \approx 1.2$) and of a high spatial resolution active coil array (4 poloidal coils $\times$ 48 toroidal coils). The new close fitting shell, installed directly over the vacuum vessel, will provide a passive boundary for both the dynamo modes and the resistive wall modes (RWMs) for times up to $\approx$50–100 ms. The new coil system will allow active control over timescales of the order of $\approx$50 ms or longer.

In comparison with the previous assembly, the modified system will have several new features. In particular,

(a) Passive stabilization of both the fast dynamics ($\tau \ll \tau_s$) of the internal dynamo resistive tearing modes and of the external kink RWM for discharges of up to $\approx$50–100 ms will be allowed.
(b) It will be possible to address the issue of active control of RWMs for discharges longer than $\approx$100 ms.
(c) With the new coil system it will be possible to produce the harmonics of the experimental MHD spectrum up to $m = 1$, $n \approx 16$, in a frequency band from DC to $\approx$50 Hz either for induced mode rotation experiments or to affect individual mode amplitude and phase.
(d) The systems offer new possibilities of feedback controlling a wide spectrum of modes for radial field minimization at the plasma boundary.

Finally, much better axisymmetric equilibrium due to the close fitting shell (Shafranov's shift $\approx$1 cm) and to the feasible dynamic equilibrium control because of the thinner shell will be possible.

With this modified assembly we plan to address several experimental topics that should contribute to a better understanding of magnetically confined plasmas and also provide precious information on the future perspectives of the RFP as a viable reactor concept. In particular, we plan to extend the study of the induced rotation of non-linearly coupled $m = 1$ and $m = 0$ modes by $m = 0$ rotating perturbations and to apply this technique also to pulsed poloidal current drive (PPCD) and oscillating poloidal current drive (OPCD) [52,53] experiments. The possibility of producing direct induced rotation of the $m = 1$ dynamo modes by $m = 1$ rotating perturbations will also be explored. Particular effort will also be devoted to the study of induced occurrence of QSH states with controllable amplitudes. The boundary conditions of the theoretical SH states imply, in fact, the existence of a continuous distribution of helical boundary currents. The existence of cuts in the shells of present RFPs prevents these currents from flowing properly and induces return currents generating MH error fields. Unless a good correction of this error field is performed, the shell acts like an ergodic divertor exciting a broad spectrum of resonant modes in the plasma core. This suggests an evolution of the RFP into a forced SH RFP where most of the helical boundary currents are provided by external windings. Such an RFP would still produce most of the confining magnetic field by plasma currents, but it would be intermediate between the tokamak (because of the toroidal current) and the stellarator (because of helical external windings).

A new category of experiments, possibly also relevant for non-RFP magnetic configurations, will be done on the active stabilization of RWMs on timescales longer than the shell time constant. In particular, by prolonging the pulse length well beyond $\approx$100 ms we will enter a regime where the shell timescale becomes significantly less than the pulse length. In this case, we should therefore be able to address thoroughly the issue of feedback control of RWMs and, if successful, demonstrate that a thick passive stabilizing shell is not necessary for the RFP.

## 8. Conclusions

Recent experimental and theoretical studies have allowed a deeper insight into the MHD properties of the RFP configuration, and, in particular, into the RFP dynamo mechanism and into the MHD instabilities behaviour. A comprehensive picture of these MHD subjects has been presented in this article, where an effort to unify various experiments and theoretical descriptions has been performed. A set of successful experiments has demonstrated the possibility of influencing both the amplitude and the spectrum of the magnetic fluctuations which characterize the RFP configuration. With these studies a reduction of magnetic chaos has been obtained. Continuous rotation of wall locked resistive tearing modes has been obtained by an $m = 0$ rotating perturbation. This perturbation induces rotation of $m = 1$ non-linearly coupled modes. Besides important information on the non-linear origin of the torque acting on the internally resonant modes, this rotation experiment proves the possibility of high current RFP operation without severe plasma–wall interaction. The simultaneous exploitation of several techniques for edge and core magnetic stochasticity reduction appears promising for the future of the RFP configuration [51]. Experiments like PPCD or OPCD have, in fact, demonstrated in principle the possibility of access to regimes with significantly enhanced confinement by active suppression of MHD instabilities.

A way to a stationary reduction of magnetic chaos has also been indicated by the discovery of experimental QSH states, where a better confined helical core is produced. It is interesting to note that SH states could be linked with the $q = 1$ mode of the tokamak and with the helical states of the stellarator. In the future the theoretical analysis should be addressed to the issue of stability, accessibility and robustness of SH states by incorporating new elements: a shell radius larger than the plasma radius, heat transport (filamentation effects might be present), the pinch parameter, the aspect ratio. In particular, linear stability theory should be developed for helically symmetric profiles. Future work should be dedicated to assessing the value of viscosity to be used in the Hartmann number so as to predict the scaling of this number towards more collisionless regimes.

Continuing along the guidelines indicated by this article, the RFX device is presently being modified. The most important modifications have been described here.

## Acknowledgements

The authors wish to dedicate this work to the memory of P. Kustatscher (who died in 2000), who gave for many years a precious and enthusiastic contribution to the RFX project.

## References

[1] Rostagni G. 1995 *Fus. Eng. Des.* **25** 301
[2] Ortolani S. and Schnack D.D. 1993 *Magnetohydrodynamics of Plasma Relaxation* (Singapore: World Scientific)
[3] Caramana E.J. *et al* 1983 *Phys. Fluids* **26** 1305
[4] Kusano K. and Sato T. 1987 *Nucl. Fusion* **27** 821
[5] Cappello S. and Biskamp D. 1996 *Nucl. Fusion* **36** 571
[6] Prager S.C. 1999 *Plasma Phys. Control. Fusion* **41** A129
[7] Terranova D. *et al* 2000 *Plasma Phys. Control. Fusion* **42** 843
[8] Valisa M. *et al* 1997 *J. Nucl. Mater.* **241–243** 988
[9] Bodin H.A.B. and Newton A.A. 1980 *Nucl. Fusion* **20** 1255
[10] Verhage A.J.L., Furzer A.S. and Robinson D.C. 1978 *Nucl. Fusion* **18** 457
[11] Sykes A. and Wesson J.A. 1977 *Controlled Fusion and Plasma Physics (Proc. 8th Eur. Conf. Prague, 1977)* vol 1 (Geneva: European Physical Society) p 80
[12] Sato T. and Kusano K. 1985 *Phys. Rev. Lett.* **54** 808
[13] Hutchinson I.H. 1984 *Plasma Phys. Control. Fusion* **26** 539
[14] Garzotti L. *et al* 2000 *Phys. Rev. Lett.* **84** 5532
[15] Fitzpatrick R. 1999 *Phys. Plasmas* **6** 1168
[16] Fitzpatrick R. *et al* 1999 *Phys. Plasmas* **6** 3878
[17] Paccagnella R. 1998 *Nucl. Fusion* **38** 1067
[18] Zanca P. *et al* 2001 *Phys. Plasmas* **8** 516
[19] Martin P. 1999 *Plasma Phys. Control. Fusion* **41** A247
[20] Escande D.F. *et al* 2000 *Phys. Rev. Lett.* **85** 1662
[21] Martin P. *et al* 2000 *Phys. Plasmas* **7** 1984
[22] Taylor J.B. 1974 *Phys. Rev. Lett.* **33** 1139
[23] Ho Y.L. *et al* 1995 *Phys. Plasmas* **2** 3407
[24] Spizzo G. *et al* 2002 *J. Nucl. Mater.* in press
[25] Zanca P. and Martini S. 1999 *Plasma Phys. Control. Fusion* **41** 1251
[26] Marrelli L. *et al* 1999 *J. Nucl. Mater.* **266–269** 877

[27] Cappello S. *et al* 1999 *Controlled Fusion and Plasma Physics (Proc. 26th Eur. Conf. Maastricht, 1999)* vol 23J (Geneva: European Physical Society) p 981
[28] Cowling T.G. 1957 *Magnetohydrodynamics* (New York: Interscience)
[29] Caramana E.J., Nebel R.A. and Schnack D.D. 1983 *Phys. Fluids* **26** 1305
[30] Aydemir A.Y. and Barnes D.C. 1984 *Phys. Rev. Lett.* **52** 930
[31] Holmes J.A. *et al* 1985 *Phys. Fluids* **28** 261
[32] Schnack D.D. 1985 *Phys. Fluids* **28** 321
[33] Kusano K. and Sato T. 1986 *Nucl. Fusion* **26** 1051
[34] Escande D.F. 2000 *Plasma Phys. Control. Fusion* **42** B243
[35] Finn J.M. *et al* 1992 *Phys. Fluids* B **4** 1262
[36] Dobrott D.D. *et al* 1985 *Bull. Am. Phys. Soc.* **30** 1399
[37] Cappello S. *et al* 1990 *Controlled Fusion and Plasma Physics (Proc. 26th Eur. Conf. Maastricht, 1999)* vol 23J (Geneva: European Physical Society) p 595 (CD-ROM file 23J)
[38] Cappello S. and Paccagnella R. 1992 *Phys. Fluids* B **4** 611
[39] Cappello S. and Paccagnella R. 1990 *Theory of Fusion Plasmas (Proc. Workshop Bologna 1990)* (Bologna: Editrice Compositori) p 595
[40] Cappello S. and Escande D.F. 2000 *Phys. Rev. Lett.* **85** 3838
[41] Montgomery D. 1992 *Plasma Phys. Control. Fusion* **34** 1157
[42] Montgomery D. 1993 *Plasma Phys. Control. Fusion* **35** B105
[43] Shan X. and Montgomery D. 1993 *Plasma Phys. Control. Fusion* **34** 619
[44] Tebaldi C. and Ottaviani M. 1999 *J. Plasma Phys.* **62** 513
[45] Escande D.F. *et al* 2000 *Phys. Rev. Lett.* **85** 3169
[46] Bartiromo R. *et al* 1999 *Phys. Rev. Lett.* **83** 1779
[47] Bartiromo R. *et al* 1999 *Nucl. Fusion* **39** 1697
[48] Chitarin G. *et al* 1999 *Plasma Physics and Controlled Fusion (Proc. 25th Eur. Conf. Prague, 1998)* vol 22C (Geneva: European Physical Society) p 766
[49] Fitzpatrick R. 1999 *Phys. Plasmas* **6** 1830
[50] Hegna C.C. 1996 *Phys. Plasmas* **3** 4646
[51] Antoni V. *et al* 2001 *Nucl. Fusion* **41** 431
[52] Bartiromo R. *et al* 1999 *Phys. Rev. Lett.* **82** 1462
[53] Bolzonella T. *et al* 2001 *Phys. Rev. Lett.* **87** 195001-1:4